An Investigation of Ammonia Primary Flame Combustor Concepts for Emissions Reduction with OH*, NH_2* and NH* Chemiluminescence at Elevated Conditions

Daniel Pugh* **Jon Runyon** **Philip Bowen** **Anthony Giles**

Agustin Valera-Medina **Richard Marsh** **Burak Goktepe** **Sally Hewlett**

Affiliation:

Cardiff School of Engineering,
Cardiff University, Wales, UK, CF24 3AA.

*Corresponding author contact details:

Email: pughdg@cardiff.ac.uk
Cardiff School of Engineering,
Cardiff University, Wales, UK, CF24 3AA
Tel. +44(0) 2920 870597

Abstract

With developing interest in NH_3 as a prospective energy carrier, combustor designs and fuelling concepts require optimisation to reduce NO_x emissions. Through the introduction of staged combustor concepts, pathways have previously been identified that limit NO_x production whilst improving combustor efficiency and reducing unburned NH_3. However, the efficacy of secondary air staging is sensitive to the primary flame behaviour, and whilst low NO_x emissions can be achieved at rich conditions, high unburned NH_3 leads to greater global NO_x concentrations from downstream production. Here, time-resolved OH*, NH_2* and NH* chemiluminescence were employed together *for the first time* for NH_3-air and NH_3-H_2-air flames to investigate a primary flame configuration that produced the lowest combined emissions concentration. A generic, fuel-flexible burner was developed to enable partial and full premixing, together with operation of a swirl-stabilised non-premixed flame. Initially, NH_3-H_2-air flames were employed in a range of configurations and produced markedly different chemiluminescence and emissions results as functions of global equivalence ratio. The performance of a pure NH_3-air flame was subsequently investigated and compared to

the blended fuel results. Optical trends complemented changes in sampled exhaust emissions, enabling analysis of intermediate chemistry. Burner inlet temperature and pressure were then increased proportionally to maintain equivalent bulk nozzle exit velocities. Contrasting trends were identified as functions of fuel composition and equivalence ratio, with a comprehensive database of optical and analytical results generated. Results obtained for NH_3-H_2-air suggest the most favourable configuration resulted from a partially premixed flame employing H_2 as a pilot, operating under rich conditions (Φ=1.2). However, at higher temperatures and pressures, the trends observed for non-premixed NH_3-air flames will lead to superior performance, particularly with a small increase in equivalence ratio.

Keywords

Ammonia, Turbulent premixed flames, Chemiluminescence, Staged combustion, Chemical kinetics

1. Introduction

With favourable storage and transportation characteristics, there is developing interest in NH_3 as a prospective energy carrier [1,2] and a cost-effective mechanism for storing H_2. The potential exists to directly supply power systems with NH_3, avoiding H_2 conversion and presenting several combustion research challenges [2-6]. NH_3 reactivity is comparatively poor, with combustion enhanced by thermolysis to form H_2 [7-9], additional supplementary fuels [8-12], or preheating. More significant is the propensity for excessive NO_x production [12-15] from fuel-bound nitrogen. Lean, low-temperature combustor strategies for NO_x reduction are ineffective for NH_3, with previous studies demonstrating successful concepts including humidification [3] and staging [14-15], alongside an increase in combustor pressure [3,16-17], making the prospective application of NH_3 more conducive to gas turbine operation.

Recent research has investigated low-NO_x NH_3 combustors [3,14,17], exploring staged concepts in detail and contrasting against CH_4-air flames [15,18]. Through the optimised introduction of staged secondary-air, pathways have been identified that limit NO_x production, whilst improving combustor efficiency through reducing unburned NH_3 [3,14,17,18]. However, detailed experimental studies with NH_3 flames remains limited, particularly at elevated inlet conditions, and an optimised primary flame configuration that provides both low NO_x and NH_3 will greatly impact the understanding and influence of downstream staging. The purpose of this study, expanding on recent findings [3], is to investigate the primary flame, exploring NO reduction pathways through the detailed optical investigation of distinct combustor concepts, and mechanisms of fuel delivery for pure NH_3 and NH_3/H_2 blends. A fuel-flexible generic swirl burner was employed in several configurations, using swirl-stabilised premixed and non-premixed NH_3-air flames, alongside partial-premixing of NH_3 and H_2. Regions of reacting OH*, NH_2* and NH* were visualised using Abel deconvoluted high-speed chemiluminescence for the first time with NH_3 flames, and compared against emissions produced. Elevated inlet conditions of temperature and pressure were subsequently investigated to indicate the change in primary flame behaviour.

2. Experimental Facility and Diagnostics

2.1 Pressurised Optical Combustor

The swirl burner employed in previous studies [3,19,20,22] was modified, as presented in the cross-sectional view in Fig.1, with a central injection lance (Fig.1a) added to facilitate fuel injection into the annular swirling flow. The lance internal diameter was sized to give approximately equal axial jet velocities (flow-path 1 in Fig. 1) to the outer swirling flow (flow-path 2) for the range of equivalence ratios specified. Premixed reactants entered the inlet plenum (Fig.1b) with all flows metered using Coriolis mass-flow control (±0.35%). The plenum body was preconditioned to the specified inlet temperature (T_x) using electric preheaters and compressed air, dried to a dew point of -17°C. From the premix chamber (Fig.1c), reactants leave the swirler exit nozzle (r=20mm) through a single radial-tangential swirler (Fig.1d) with a geometric swirl number of S_g=0.8, using the central injection lance as a bluff-body. Quartz windows (Fig.1e) allowed optical access into a high-pressure optical casing (Fig.1g) with high-speed chemiluminescence measurements taken perpendicular to the reactant flow direction. The flame was housed within cylindrical quartz confinement (Fig.1f) at an expansion ratio of 2.5 from the nozzle. The system was pressurised to each specified condition (P_x) using a water-cooled back-pressure valve. Greater detail of the experimental setup is provided in other works [19-20,22].

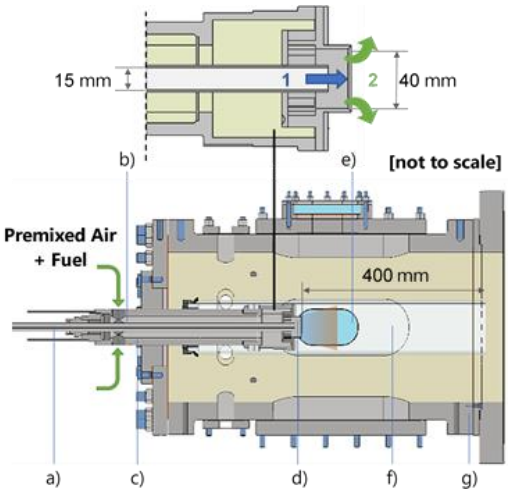

Fig.1 Burner assembly

2.2 Emissions

Combustor exhaust gas emissions were sampled downstream of the quartz confinement using a 9-hole equal-area probe, water-conditioned with a heat exchanger to regulate sample temperature (433K) following specifications in ISO-11042 [21]. The pump, filter block and sample lines were also maintained at 433K. NO_x (NO and NO_2) concentrations were quantified using heated vacuum chemiluminescence (Signal 4000VM). Unburned NH_3 measurements were obtained by redirecting sample through an NO converter (Signal 410) to measure unreacted concentrations (80% conversion efficiency). All NH_3 and NO_x concentrations were measured hot/wet and normalised to equivalent dry conditions (Eqn. (9) in ISO-11042). Dry O_2 concentrations were quantified using a paramagnetic analyser (Signal 9000MGA) and used to subsequently normalise NO_x to equivalent 15% O_2 (Eqn. (10) in ISO-11042). After changing experimental conditions, burner temperatures, pressures, flows and emissions were monitored and, once stable, held for a minimum of 60 samples to be taken. Systematic uncertainties comprising analyser specification, linearisation and span gas certification were combined with any fluctuations in measurement to give the total uncertainty represented by the plotted error bars.

2.3 Chemiluminescence

Time-resolved chemiluminescence measurements were conducted at each experimental condition, targeting three electronically-excited intermediate chemical radicals within NH_3-air and NH_3-H_2-air flames, namely OH*, NH_2* and NH*. These measurements were taken utilising a combination of Phantom v1212 high-speed CMOS camera, Specialised Imaging SIL40HG50 high-speed image intensifier, UV lens (78 mm, f/11), and narrow bandpass filters selected specifically for each radical species. Further information on this specific high-speed imaging setup is found in other works [22]. While the authors have previously conducted OH* chemiluminescence measurements in NH_3-based flames [3,12], focusing specifically on the well-known $A^2\Sigma^+$–$X^2\Pi$ OH* system [23] using a 315 nm (±15 nm FWHM) bandpass filter as in this study, only a select few experimental studies have conducted NH_2* and NH* chemiluminescence measurements, typically confined to canonical reactors [24-27] or shock tubes [28-29] rather than premixed or diffusion NH_3 swirl flames, where NH_2 and NH intermediate chemistry is key to NH_3 oxidation [1-3]. For NH_2* measurements in this

study, a single peak of the NH_3 α band was selected at 630 nm [23,26] using a bandpass filter centred at 632 nm (±10 nm FWHM). For NH* measurements, the $A^3\Pi–X^3\Sigma^-$ system was selected at 336 nm [23-25, 27-29] using a bandpass filter centred at 337 nm (±10 nm FWHM). Filter specifications provide nominal values, however filter transmission curves encompass expected OH*, NH*, and NH_2* wavelengths with minimal overlap. Transmission of the NH* filter below 327 nm is <0.1%, well away from the 309 nm OH* peak. At the peak NH* wavelength of 336 nm, the OH* filter transmittance is ~1%. H_2O interference in the NH_2* signal was expected to be minimal as shown in [30]. The system was calibrated for the spectral efficiencies of both camera and intensifier, alongside the employed filters, UV lens, and optical windows. The transmission efficiency ratios of OH*/NH_2* and NH*/NH_2* were respectively calculated as 1.9:1 and 5.7:1 at peak emission wavelengths, with further detail included in supplemental material.

The frame rate deployed was 4000 Hz, with the image intensifier gated at 10μs and the intensifier gain held constant throughout. A scaled target image provided the image resolution, equal to 4.6 pixels/mm, resulting in a field of view of 75mm (axial, y) by 100mm (radial, x) relative to the edge and centreline of the burner exit nozzle, respectively. For images presented herein, each instantaneous chemiluminescence image was filtered using a 3x3 pixel median filter and temporally averaged from 2000 images. The temporally-averaged images were then background corrected and processed using a modified Abel inversion algorithm to provide an axisymmetric planar representation of the electronically-excited radical species distribution within the swirling flow field [31]. Quantification of the chemiluminescence signal was further conducted using an integral intensity, e.g. II_{OH*} as described by Runyon et al. [31].

Proportionality between electronically excited and ground state species with the spectroscopic flame response is complicated by influences such as radiation losses and quenching. Previous works have employed a directly proportional response relating NH* to NH and NH_2* to NH_2 in NH_3 dissociation [32], however proportionality is not assumed in this paper. Instead, only a positive correlation between emitting

and ground state radicals is applied, and that more emitting species suggests increased ground state population [29,33,34].

3. Experimental Specification

Initial experiments were undertaken using a 70/30%$_{vol}$ ratio of NH_3-H_2, having demonstrated favourable stability in previous work [3] and shown to exhibit comparable behaviour to CH_4-air [35]. A fully premixed flame was obtained by directing all reactants to the outer swirling flow (flow-path 2 - Fig.1). The fuel streams were then separated for the partially premixed configuration, with H_2 directed to the central diffusion jet (flow-path 1 - Fig.1) and NH_3 premixed with air in the outer swirling airflow (arrangement denoted 'H_{2Diff}'). H_2 and NH_3 were subsequently interchanged, with the former directed to the swirling premixed flow ('NH_{3Diff}'). Data-points were specified for a change in global equivalence ratio (Φ=0.9-1.2) by varying the swirling air flow rate with each flame configuration, capturing emissions and optical data. It should be noted that changing Φ will provide small changes in swirl/recirculation, and whilst flow field effects are unquantified, changes in flame shape are visualised via chemiluminescence. Baseline inlet conditions of temperature (T_1) and pressure (P_1) were specified at 323K and 0.11MPa. Ambient conditions were elevated with a constant T/P ratio, retaining quasi-steady nozzle outlet velocities and combustor residence time for each configuration and Φ. The elevated temperature conditions were specified as 411K and 499K (T_2, T_3), corresponding to respective elevated-inlet pressures of 0.14MPa and 0.17MPa (P_2, P_3). Taking the stoichiometric fully premixed case as an example; swirler nozzle bulk outlet velocities were maintained with Reynolds numbers reducing from ~15,200 at T_1/P_1, to ~11,200 at T_3/P_3. H_2 supply was subsequently removed and a comparison made between premixed/non-premixed NH_3-air flames, with fuel-flow increased to maintain a constant net thermal power of 25kW$_{th}$ – equivalent to the NH_3-H_2 case (based on proportional fuel LHV). Whilst significant results are presented and discussed, the full experimental dataset of inlet conditions and results is provided in the supplemental material.

3.1 Chemical Kinetics Modelling

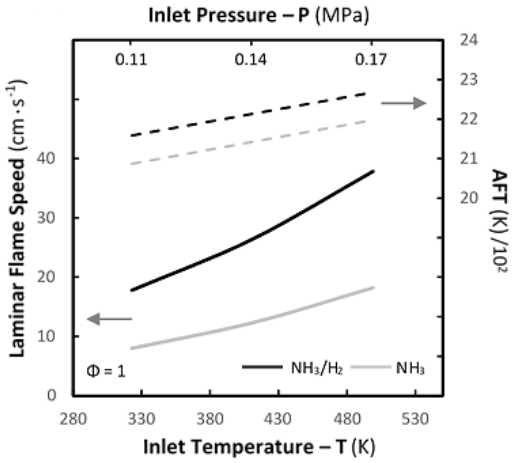

Fig.2 Changes in modelled S_L (solid) and AFT (dotted) for each fuel at the specified conditions (Φ=1)

Chemical kinetics were modelled using CHEMKIN-PRO, with the PREMIX reactor used to simulate changes in laminar flame speed (S_L). Solutions were based on an adaptive grid, with multi-component transport properties and new schemes for convective flux. The equilibrium tool was used to generate adiabatic flame temperatures (AFT), under conditions of constant pressure/enthalpy. Each simulation employed the NH_3 reaction mechanism from Okafor et al. [11] comprising 59 chemical species and 356 reactions. Changes in S_L and AFT are shown at Ø=1 and changing T/P in Fig.2, for the premixed NH_3-air and NH_3-H_2-air cases. Even at the lowest inlet temperatures, AFT is sufficient to facilitate thermal NO_x formation [36] and was shown to vary by ~80K across the specified experimental range for both fuel mixtures. Pure NH_3-air flame temperatures were ~70K lower than each equivalent NH_3-H_2-air condition. The low S_L for NH_3 is highlighted in Fig. 2 and is predicted to approximately double with the addition of 30% H_2 for all equivalent cases of T/P. The highest S_L at T_3/P_3 highlighted the potential for flashback with NH_3-H_2-air and relatively low nozzle velocities.

4. Results

4.1 NH_3-H_2-air flames

Sampled concentrations of NO and NH_3 from the fully premixed, H_{2Diff}, and NH_{3Diff} flames are shown in Fig. 3 for change in Φ at T_1/P_1. NO_2 is not plotted - or NH_3 for the premixed case - as measured concentrations were negligible compared to NO; the data is provided in the supplemental material. Note - lean premixed CH_4/air in the same facility gave ~5-30 $ppmvd_{15\%O2}$.for an AFT range of ~1800-2200K [22]. A near order of magnitude increase in NO concentration produced by the premixed flame is observed, compared to the NH_{3Diff} regime. Local NH_3-rich zones lead to increased production of NH_2* within the NH_{3Diff} flame, as evidenced in the Abel-transformed chemiluminescence shown in Fig.4 (Φ=1) - one half of the planar representation is shown, with x= 0 corresponding to the burner centreline and flow from the bottom up. Measured intensities of NH_2* were significantly higher than both OH* and NH* (even accounting for the increase in quantum efficiency with the UV-enhanced photocathode of the intensifier), though with the colourmap presented, profiles are normalised to the maximum in each image to show the change in topology for each configuration. Each flame stabilises along the shear layer of zero axial velocity [19,22], with the flame brush thicker and structure markedly different for the partially premixed cases. Significantly greater NH_2* intensities were evident post-flame for the NH_{3Diff} case, when compared to

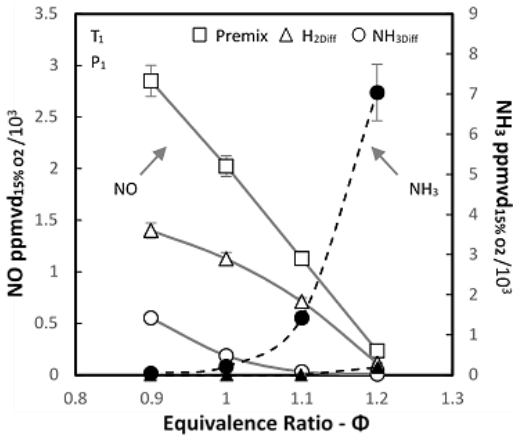

Fig.3 Sampled NO (empty) and NH_3 (filled) emissions for each NH_3-H_2 flame configuration at T_1/P_1

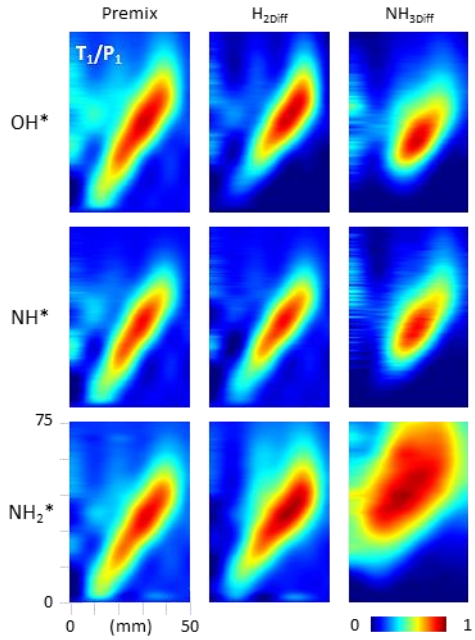

Fig.4 Abel transformed NH*, OH* and NH_2* chemiluminescence for each NH_3-H_2 flame configuration at T_1/P_1.
(colourmap normalised to image max)

the other regimes. NH_2 is noted as being key for enhancing NO consumption through the chain carrying reaction $NH_2+NO\leftrightarrow NNH+OH$, and the terminating reaction $NH_2+NO\leftrightarrow H_2O+N_2$ [3]. OH and O are also important for the respective oxidation of NH and NH_2 to NO via HNO and the reaction $HNO+OH\leftrightarrow NO+H_2O$ [2]. With a positive correlation between ground state and excited species, enhanced NH_2* and reduced regions of OH* evident in Fig.4 complement the reduction in NO concentrations shown in Fig. 3 for the NH_{3Diff} case. The change in each chemiluminescence intensity distribution was quantified by calculating the integral intensity [31] for each species, with values of II_{NH2*} for NH_{3Diff} a factor of 3.7 greater than the equivalent premixed flame. The H_{2Diff} flame behaves as an intermediate between the other two configurations, with NH_2*and OH* chemiluminescence profiles demonstrating transitional behaviour as seen with measured NO. The distribution of NH* appears to closely match the deconvoluted OH* profiles, while ground state OH and NH are related by the primary production pathway: $NH_2+OH\leftrightarrow NH+H_2O$.

A pronounced decrease in NO with increasing Φ is also evident in Fig. 3, as previously observed [3]. This results from a combination of reduced thermal formation with the Zel'dovich mechanism, the availability of OH for NH_3 oxidation [16,18], and enhanced NO consumption with NH_2. Figure 5 shows the change in OH* and NH_2* chemiluminescence profiles for a sample H_{2Diff} flame with change in Φ at T_2/P_2. The colourmaps in these images have been normalised to the maximum for each species dataset to emphasise the change in excited radical intensity with Φ. A complementary trend is seen again between the reduction of OH*, an increase in NH_2* intensity, and a drop in NO (data shown for T_2/P_2 in Fig. 6). As modelled in Section 3.1, AFT is highest for the Φ=1 case, and expected to reduce by ~80K to near equivalent values for both Φ=0.9 and 1.2. The influence of rising AFT was investigated in further detail, by increasing T_1/P_1 to T_3/P_3. The change in sampled NO concentrations for each NH_3-H_2-air flame configuration is plotted

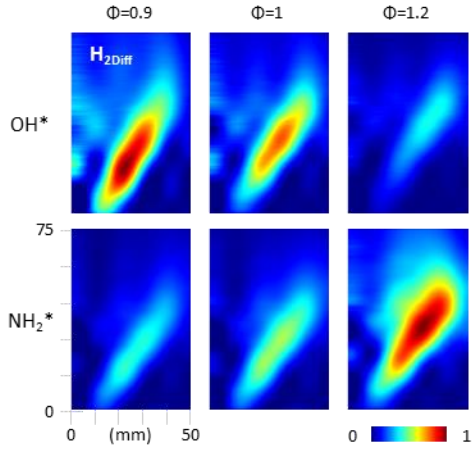

Fig.5 Abel transformed OH* and NH_2* chemiluminescence for the H_{2Diff} flame configuration at T_2/P_2
(colourmap normalised to species dataset max)

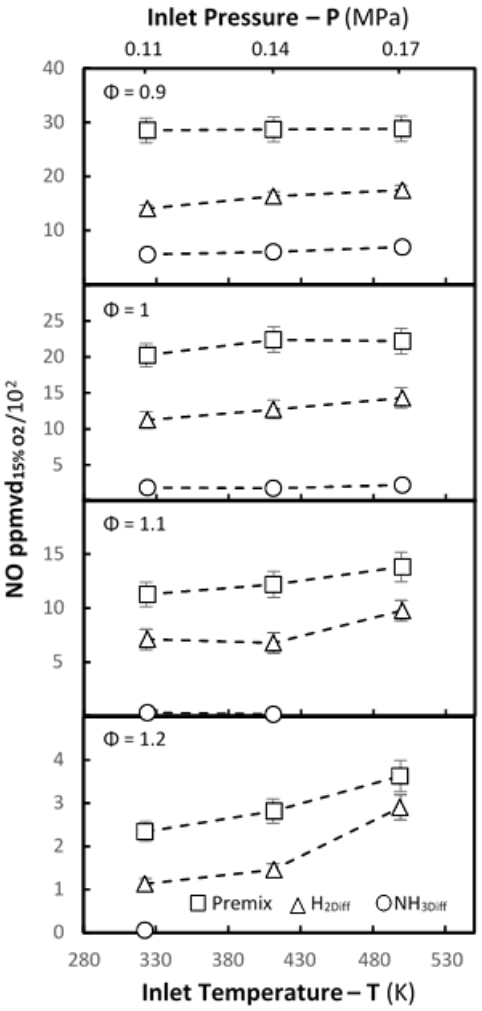

Fig.6 Sampled NO emissions for each NH_3-H_2 flame configuration and Φ at elevated inlet conditions

against increasing inlet conditions in Fig. 6, for distinct Φ. The observed trend is for increased NO production with inlet temperature, as would be expected from enhanced thermal NO_x formation. However, this is diminished due to the NO reduction induced by rising inlet pressure – resulting in increased NH_2 from HNO/OH and third-body H_2O production from OH, as has been previously shown for NH_3-H_2-air flames by the authors [3]. This pressure effect is seemingly overcome by enhanced OH production at elevated temperature through $H+O_2 \leftrightarrow O+OH$ and $2OH \leftrightarrow O+H_2O$, and increased Zel'dovich production via $N+O_2 \leftrightarrow NO+O$ and $N+OH \leftrightarrow NO+H$ [36] - taking Φ=1 as an example, Zel'dovich reaction rates were simulated to rise by factors of ~3 with the specified elevation in conditions (note - Kobayashi et al. [2] demonstrated effective NO consumption via $N_2+O \leftrightarrow NO+N$ for NH_3-air flames). The relative trends observed in Fig. 6 appear to be more pronounced at richer conditions; as for the leaner cases OH fractions are higher so enhanced NO production from rising temperature is diminished. It should be emphasised, the decoupled dominant reactions highlighted for changes in NO formation with temperature and pressure have been reported for NH_3-H_2 flames [3,9,14], and this work was specified to highlight that influences are competing as T/P increase together as may be expected with practical systems. A comparison between changes in OH* and NH_2* chemiluminescence is shown in Fig.7 for the Φ=1 NH_{3Diff} flame and increasing T/P. To demonstrate the differences in flame topology and chemiluminescence intensity with T/P, colourmaps are normalised to the maximum in both species' dataset (Fig.7a) and each image (Fig.7b). The OH* and NH_2* chemiluminescence intensities are shown to rise with increasing temperature and pressure. However, the flame structure is also

shown to contract with increasing inlet conditions (Fig.7b). This results from enhanced reactivity from increasing temperature, and the reduction in flame thickness induced from increasing pressure. It should be noted the increase in collisional quenching resulting from a rise in pressure would be expected to reduce observed chemiluminescence [33,37], however the inverse is observed resulting from increased production from changes in intermediate chemistry and an increase in flame temperature. Emissions data could not be collected at the richest conditions for the NH_{3Diff} flame at elevated temperature and pressure – the reduction in outlet velocities with decreasing airflow led to a change in flame mode, and effective flashback into the burner nozzle with premixed H_2. To sustain a rich NH_{3Diff} flame at elevated conditions an increase in nozzle outlet velocity is required, and therefore thermal power; this is outside the scope of this study. The NH_{3Diff} flame produced significantly higher NH_3 emissions than the other two configurations, rising with increasing Φ. This is simulated to primarily result from the elevated NH_2 concentrations, with the respective third body and branching reactions $NH_2+H+M \leftrightarrow NH_3+M$, and $2NH_2 \leftrightarrow NH_3+NH$. With the change in experimental configuration, there exists the potential for fluid dynamic influences to contribute to enhanced exhaust NH_3, however measured exhaust O_2 concentrations at stoichiometric conditions were similar for all flame configurations and T/P, suggesting sufficient mixing of reactants. Excessive NH_3 emissions from the primary flame will lead to increased aggregate NO_x production in a staged configuration. Whilst the NH_{3Diff} flame provided the lowest NO emissions, NH_3 concentrations meant that optimal (combined NO and NH_3) performance was achieved with the H_{2Diff} flame at Φ =1.2, with a marginal difference compared to the fully premixed case.

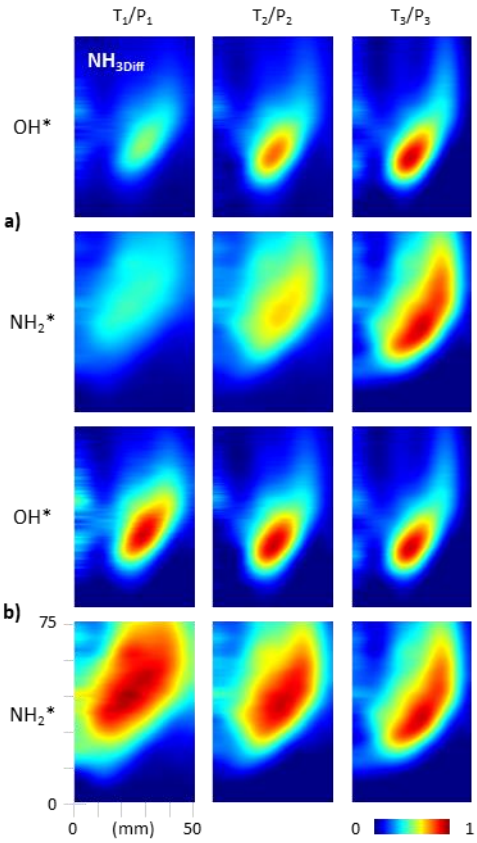

Fig.7 Abel transformed OH* and NH_2* chemiluminescence for the Φ=1 NH_{3Diff} flame configuration for increasing inlet conditions. (colourmaps normalised to species dataset max (a) and image max (b))

4.2 NH_3-air Flames

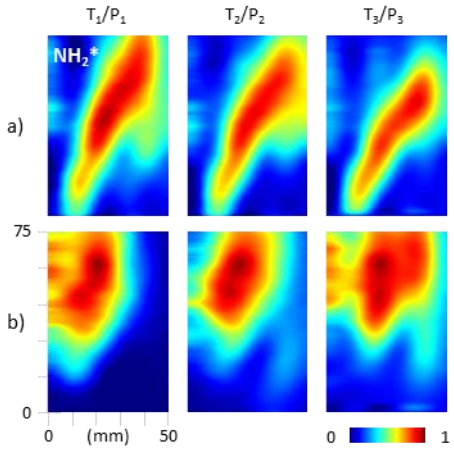

Fig.8 Abel transformed NH_2* chemiluminescence for the Φ=1 NH_3-air with premixed (a) and non-premixed (b) flames
(colourmaps normalised to image max)

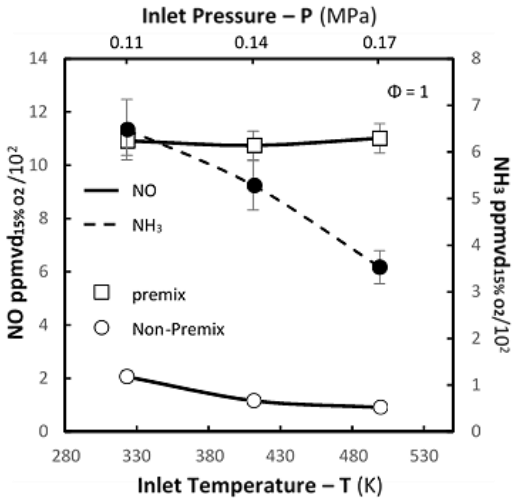

Fig.9 Sampled NO (empty) and NH_3 (filled) emissions for each NH_3-air flame configuration with increasing inlet condition

For practical systems there are advantages of operating with NH_3-air flames only. Hence, further studies were undertaken with both non-premixed and premixed configurations (respective fuel flow paths 1 and 2 in Fig.1). At lower temperatures, ignition could not be achieved with NH_3/air alone, and H_2 addition was required. The H_2 was subsequently removed after flame stabilisation. At T_3, the stoichiometric NH_3-air flame ignited in both configurations without H_2 addition. A comparison of Abel transformed NH_2* chemiluminescence from Φ=1 premixed and non-premixed NH_3-air flames is shown in Fig. 8. For the premixed regime, as inlet temperature and pressure rise, the flame compresses, retreating upstream in the flow and expanding radially – as would be expected with increased reactivity and reduced flame thickness, with NH_2* chemiluminescence in the outer recirculation zones reduced Conversely, for the non-premixed case, higher NH_2* intensities initially appear near the centreline, then as T increases, NH_2* within the flame brush radially thickens and higher intensities are established in the outer recirculation zone. These opposing trends are matched in the emissions data shown in Fig. 9. With an increase in T/P, the premixed NH_3-air flame exhibits the same behaviour as NH_3-H_2-air, and gives a small increase in NO. For the non-premixed flame however, NO is shown to approximately halve across the specified range. In the premixed case it is suggested that enhanced mixing leads to increased OH production at elevated conditions, supported by kinetic modelling

and chemiluminescence (available in the full dataset). However, for the non-premixed case reduced relative OH production allowed the NH_2/pressure effect (described in the section 4.1) to dominate. There is also a noticeable reduction in NH_3 emissions with an increase in T/P for the non-premixed case (premixed case not presented as concentrations were negligible). This is modelled to result from a switch in the $NH_3+H \leftrightarrow NH_2+H_2$ reaction, producing NH_3 at lower temperatures and reversing to consume it with a rise in temperature. This also contributes to the enhanced production of NH_2 and reduction in NO.

5. Conclusions

A combination of time resolved OH*, NH_2* and NH* chemiluminescence was employed for the first time with NH_3 flames. The optical techniques were used to investigate a primary flame configuration that produced the lowest combined concentrations of NO and NH_3 for two fuels: pure NH_3 and NH_3/H_2 (70/30%vol). Results highlighted that NH_2* intensity is a good marker for NO consumption in rich NH_3 flames. Measured intensities elucidated changes in sampled exhaust emissions, supporting detailed analysis of intermediate chemistry.

A generic, fuel-flexible burner was developed that enabled partial and full premixing of fuels, together with a swirl-stabilised diffusion flame. The facility was used with a combination of NH_3-H_2-air flames, with markedly different results obtained for each configuration as a function of Φ. Partial premixing of H_2, with non-premixed NH_3, provided to the lowest measured NO concentrations, an order of magnitude below the fully premixed case, but also produced more unburned NH_3. The performance of a pure NH_3-air flames was also investigated, showing an order of magnitude reduction in NO between premixed and non-premixed configurations.

Conditions of temperature and pressure were scaled in proportion to maintain equivalent bulk nozzle exit velocities with contrasting trends identified as functions of fuel composition and Φ: For NH_3-H_2-air flames, an increase in T/P led to a rise in measured NO. However, across the specified range, NO concentrations halved for non-premixed NH_3-air and reached lower NO concentrations than any other stoichiometric case.

To optimise the primary flame for staged combustion, the lowest combination of NH_3 and NO was achieved as a function of equivalence ratio. Previous studies have suggested Φ=1.2-1.3 for premixed flames, or mildly rich (Φ=1-1.1) for diffusion [3,15,17,19]. Results obtained for NH_3-H_2-air suggest the most favourable configuration resulted from the partially premixed H_{2Diff} flame with the lowest combination of NO and NH_3 achieved at Φ=1.2. It is acknowledged that at higher temperatures and pressures, the trends observed for the non-premixed NH_3 flame will lead to superior performance, particularly with a small increase in Φ, and will be the subject of future study.

Acknowledgements

This work was supported by the FLEXIS project with funding from the Welsh European Funding Office. The research was undertaken at the Cardiff University's GTRC with invaluable technical support from Steve Morris and Jack Thomas, and the data underpinning the results presented here can be found at http://doi.org/10.17035/XXXXXXXXXXXXXX.

References

[1] A. Valera-Medina, H. Xiao, M. Owen-Jones, W. David, P. Bowen, Ammonia for power, Prog. Energ. Combust. Sci. 69 (2018) 63-102.

[2] H. Kobayashi, A. Hayakawa, K.D.K. A. Somarathne, E. C. Okafor, Science and technology of ammonia combustion, Proc. Comb. Inst. 37 (1) (2019) 109-133.

[3] D. Pugh, et al. Influence of steam addition and elevated ambient conditions on NO_x reduction in a staged premixed swirling NH_3/H_2 flame, Proc. Comb. Inst. 37 (4) (2019) 5401-5409.

[4] U.J. Pfahl, M.C. Ross, J.E. Shepherd, K.O. Pasamehmetoglu, C. Unal, Flammability limits, ignition energy, and flame speeds in H_2–CH_4–NH_3–N_2O–O_2–N_2 mixtures, Combust. Flame 123 (2000) 140-158.

[5] A. Hayakawa, T. Goto, R. Mimoto, Y. Arakawa, T. Kudo, H. Kobayashi, Laminar burning velocity and Markstein length of ammonia/air premixed flames at various pressures, Fuel 159 (2015) 98-106.

[6] O. Mathieu, E.L. Petersen, Experimental and modeling study on the high-temperature oxidation of Ammonia and related NO_x chemistry, Combust. Flame 162 (2015) 554-570.

[7] H. Nozari, G. Karaca, O. Tuncer, A. Karabeyoglu, Porous medium based burner for efficient and clean combustion of ammonia–hydrogen–air systems, Int. J. Hydrogen Energ. 42 (21) (2017) 14775-14785.

[8] M. Guteša Božo, MO. Vigueras-Zuniga, M. Buffi, T. Seljak, A. Valera-Medina, Fuel rich ammonia-hydrogen injection for humidified gas turbines, Appl. Energ. 251 (2019) Volume 251, 113334.

[9] A. Valera-Medina, et al. Premixed ammonia/hydrogen swirl combustion under rich fuel conditions for gas turbines operation, Int. J. Hydrogen Energ. 44 (2019) 8615-8626.

[10] O. Kurata et al. Performances and emission characteristics of NH_3–air and NH_3CH_4–air combustion gas-turbine power generations Proc. Comb. Inst. 36 (3) (2017) 3351-3359.

[11] E. C. Okafor et al. Experimental and numerical study of the laminar burning velocity of CH_4–NH_3–air premixed flames, Combust. Flame 187 (2018) 185-198,

[12] A. Valera-Medina, et al. Ammonia–methane combustion in tangential swirl burners for gas turbine power generation, Appl. Energ. 185 (2) (2017) 1362-1371.

[13] A. Hayakawa, et al. Experimental investigation of stabilization and emission characteristics of ammonia/air premixed flames in a swirl combustor, Int. J. Hydrogen Energ. 42 (19) (2017) 14010-14018.

[14] O. Kurata, et al. Development of a wide range-operable, rich-lean low-NO_x combustor for NH_3 fuel gas-turbine power generation, Proceedings of the Combustion Institute, Proc. Comb. Inst. 37 (4) (2019) 4587-4595.

[15] K. D. K. A. Somarathne et al. Emission characteristics of turbulent non-premixed ammonia/air and methane/air swirl flames through a rich-lean combustor under various wall thermal boundary conditions at high pressure, Combust. Flame 210 (2019) 247-261.

[16] K. Somarathne, S. Hatakeyama, A. Hayakawa, H. Kobayashi, Numerical study of a low emission gas turbine like combustor for turbulent ammonia/air premixed swirl flames with a secondary air injection at high pressure Int. J. Hydrogen Energ. 42 (44) (2017) 27388-27399.

[17] E. C. Okafor, et al. Towards the development of an efficient low-NO_x ammonia combustor for a micro gas turbine, Proc. Comb. Inst. 37 (4) (2019) 4597-4606.

[18] E. C. Okafor, et al. Control of NO_x and other emissions in micro gas turbine combustors fuelled with mixtures of methane and ammonia, Combust. Flame, 211 (2020) 406-416.

[19] D. Pugh et al. Dissociative influence of H_2O vapour/spray on lean blowoff and NO_x reduction for heavily carbonaceous syngas swirling flames, Combust. Flame 177 (2017) 37-48.

[20] D. Pugh et al. Catalytic Influence of Water Vapor on Lean Blow-Off and NO_x Reduction for Pressurized Swirling Syngas Flames, J. Eng. Gas Turbines Power, 140 (6) (2018) 061502.

[21] British Standard ISO 11042-1:1996, Gas turbines. Exhaust gas emission Measurement and evaluation, British Standards Institution, U.K. (1996).

[22] J. Runyon et al. Characterization of ALM Swirl Burner Surface Roughness and Its Effects on Flame Stability Using High-speed Diagnostics J. Eng. Gas Turbines Power 142 (4) 2020, 041017.

[23] A. G. Gaydon, The Spectroscopy of Flames, 2nd Edition. Chapman and Hall. London U.K. 1974.

[24] A. Fontijn, Mechanism of CN and NH Chemiluminescence in the N–O–C_2H_2 and O–NO–C_2H_2 Reactions J. Chem. Phys. 43, (1965)

[25] A. Burgeat et al. roduct Branching Ratios of the CH + NO Reaction, J. Phys. Chem. A, 102 (42) (1998) 8124-8130.

[26] Y. Yi et al. Plasma-Triggered CH_4/NH_3 Coupling Reaction for Direct Synthesis of Liquid Nitrogen-Containing Organic Chemicals, ACS Omega, 2 (12) (2017) 9199-9210

[27] K. Ohashi et al. Alignment dependence of the amidogen chemiluminescence in the reaction of argon(3P) atoms with the aligned ammonia molecules, J. Phys. Chem. 93 (14) (1989) 5484-5487

[28] Schott et al. Exploratory shock-wave study of thermal nitrogen trifluoride decomposition and reactions of nitrogen trifluoride and dinitrogen tetrafluoride with hydrogen J. Phys. Chem. 77 (24) (1973) 2823-2830

[29] T.R. Roose, R.K. Hanson, C.H. Kruger, A shock tube study of the decomposition of no in the presence of NH_3, Proc. Comb. Inst. 18 (1) (1981) 853-862.

[30] A. Hayakawa et al. NO formation/reduction mechanisms of ammonia/air premixed flames at various equivalence ratios and pressures, Therm. Eng. Pow. Eng. 2 (2015) 14-00402.

[31] J. Runyon et al. Lean methane flame stability in a premixed generic swirl burner: Isothermal flow and atmospheric combustion characterization, Exp. Therm. Fluid Sci. 92 (2018) 125-140.

[32] R. d'Agostino et al. Kinetic and spectroscopic analysis of NH_3 decomposition under R.F. Plasma at moderate pressures, Plasma Chem. Plasma Process. 1 (1981) 19-35.

[33] J. Ballester et al. Diagnostic techniques for the monitoring and control of practical flames, Prog. Energ. Combust. Sci. 36 (2010) 375-411.

[34] S. Sheehe and S. Jackson, Spatial distribution of spectrally emitting species in a nitromethane–air diffusion flame and comparison with kinetic models, Combust. Flame 213 (2020) 184-193.

[35] F.J. Verkamp, M.C. Hardin, J.R. Williams, Ammonia combustion properties and performance in gas-turbine burners, Proc. Comb. Inst. 11 (1) (1967) 985-992,

[36] C.K Law, Combustion physics, Cambridge University Press, U.K. (2006) p.109-113.

[37] T.Kathrotia et al. Study of the H + O + M reaction forming OH∗: Kinetics of OH∗ chemiluminescence in hydrogen combustion systems, Combust. Flame 157 (2010) 1261-1273.

Figure Captions

Fig.1 Burner assembly

Fig.2 Changes in modelled S_L (solid) and AFT (dotted) for each fuel at the specified conditions (Φ=1)

Fig.3 Sampled NO (empty) and NH_3 (filled) emissions for each NH_3-H_2 flame configuration at T_1/P_1

Fig.4 Abel transformed NH*, OH* and NH_2* chemiluminescence for each NH_3-H_2 flame configuration at T_1/P_1. (colourmap normalised to image max)

Fig.5 Abel transformed OH* and NH_2* chemiluminescence for the H_{2Diff} flame configuration at T_2/P_2 (colourmap normalised to species dataset max)

Fig.6 Sampled NO emissions for each NH_3-H_2 flame configuration and Φ at elevated inlet conditions

Fig.7 Abel transformed OH* and NH_2* chemiluminescence for the Φ=1 NH_{3Diff} flame configuration for increasing inlet conditions. (colourmaps normalised to species dataset max (a) and image max (b))

Fig.8 Abel transformed NH_2* chemiluminescence for the Φ=1 NH_3-air with premixed (a) and non-premixed (b) flames (colourmaps normalised to image max)

Fig.9 Sampled NO (empty) and NH_3 (filled) emissions for each NH_3-air flame configuration with increasing inlet condition

Supplemental Material

Experimental data